Design of a horizontal axis marine current turbine with dedicated hydrofoil sections

Francisco Espenica, Ricardo B. Santos Pereira, João Baltazar and José A.C. Falcão de Campos

Abstract—**The present study describes the planform design of a full-scale turbine using a lifting line theory-based method. A full-scale reference turbine based on Bahaj's experimental model is initially designed and used for comparison, with rotor blades composed of reference sections NACA 63-824, 63-821, 63-818, 63-815 and 63-812, from root to tip. The foil sections are studied in terms of hydrodynamic and cavitation performance with the subsonic foil analysis software XFOIL. In order to mimic real marine turbine operating conditions, the critical factor controlling laminar-turbulent transition is set at N_{crit}= 4. The turbine design conditions are tip speed ratio TSR of 6 and rated speed U_0 of 2 m/s, resulting in an expected power coefficient C_P of 0.484. Subsequently, the reference turbine is redesigned using the same lifting-line method but employing a set of dedicated (hydro) foil sections from the IST-MT1-XX series. The geometry of the final, redesigned turbine is derived in a two-step approach: first a hydrodynamically optimized turbine is obtained which maximizes power extraction, increasing the power coefficient by 0.3% at design conditions and reducing the blade chord up to 41%, compared to the full-scale reference turbine; finally the chord and pitch distribution are adjusted in order to ensure structural integrity while maintaining the optimized hydrodynamic loading distribution. This procedure leads to a final geometry which maintains the reference turbine's performance while reducing the chord up to 27%. Future studies should integrate foil and blade design to further increase hydrodynamic performance and include a more comprehensive load analysis to ensure structural feasibility.**

Keywords – **tidal energy, marine current, marine turbine, design**

I. Introduction

As part of the worldwide objective of increasing renewable energy penetration in the energy production mix [1], considerable research effort has been made in recent years in the area of ocean energy. [2].

ID: 1629, track: THM
This work was supported by FCT/MCTES (PIDDAC) through project UID/EEA/50009/2019
F. Espenica was with Instituto Superior Técnico (IST) as MSc researcher, Av. Rovisco Pais, 1, 1049-001, Lisboa (email: francisco.espenica@tecnico.ulisboa.pt)
R.B. Santos Pereira is an assistant professor at IST, Av. Rovisco Pais, 1, 1049-001, Lisboa, and TUDelft, Mekelweg 5, 2628 CD Delft, Netherlands (email: ricardosantospereira@tecnico.ulisboa.pt)
J. Baltazar is a researcher at IST, Av. Rovisco Pais, 1, 1049-001, Lisboa (email: joao.baltazar@ist.utl.pt
J. A. C. Falcão de Campos is associate professor at IST, Av. Rovisco Pais, 1, 1049-001, Lisboa (email: falcao.campos@tecnico.ulisboa.pt)

Different types of energy can be extracted from the ocean, such as thermal, ocean osmosis (salinity gradients), biomass, wave energy (power harnessed from wind driven waves) and hydro-kinetic energy (extraction of kinetic energy from current motion), being the last two the main focus of recent research [3]. Among these, hydro-kinetic energy and more specifically the extraction of kinetic energy from currents generated by tidal motion is more advantageous due to the high predictability of its source [4]. The horizontal-axis current turbine (HACT) appears to be the most technologically and economically viable current harnessing technology presently available [5],[6].

With these considerations in mind, the present study aims to: 1 - design the planform of a full-scale reference turbine based upon a previous experimental model [7] to use as a means of comparison; and 2 - redesign the turbine geometry by incorporating dedicated hydrofoil sections. The present article was developed in close connection with [8] and [9].

Section II describes the design of the geometry of the full-scale reference turbine, including a sensitivity study on the influence of factor N_{crit} on hydrofoil performance and the calculation of turbine operating curves. Section III describes the redesigned turbine, obtained in a two-step approach. Finally section IV states the main conclusions study and provides an outlook for future studies.

II. Reference Turbine

This section describes the design of a full-scale reference turbine, based on the experimental model of Bahaj et al. [7]. The planform of the full-scale reference turbine is designed using a lifting line theory-based method [9],[10],[11], from which an optimal blade chord and twist distribution are obtained. The foil relative thickness (t/c) spanwise distribution and blade profiles are the same as in the model turbine. The blade sections are NACA 63-824, 63-821, 63-818, 63-815 and 63-812, from root to tip, respectively.

A. N_{crit} factor influence on foil performance

Since the software XFOIL [12] is used to estimate the hydrodynamic performance of the blade sections, which in turn depends on the N_{crit} factor, a sensitivity study is carried out. This factor is the exponent in what is called the e^n method, which has been widely used since its introduction in 1956 by Smith et al. [13] as the method to directly model the growth of Tollmien-Schlichting waves in the boundary layer, shown by Schubauer et al. [14] to be

the precursor to transition in a low-turbulence environment. Implemented in XFOIL, the user-specified parameter N_{crit} is the logarithm of the amplification factor of the most-amplified frequency which triggers transition. The value of this parameter depends on the ambient disturbance level in which the foil operates and mimics the effect of such disturbances on transition [13].

The NACA 63-815 section at Reynolds number of $1{\cdot}10^6$, $5{\cdot}10^6$, $1{\cdot}10^7$ and $2{\cdot}10^7$ is considered. This particular foil is selected for the sensitivity study because it is the section located at the reference turbine's relative radial position r/R = 0.75 and may thus be considered representative of the overall performance. The value of 9 corresponds to the standard value for N_{crit} [13], emulating the conditions in an average wind tunnel. N_{crit} = 1 corresponds to a situation in which flow disturbances are very large, precipitating transition almost instantly. N_{crit} = 4 is an intermediate value between 1 and 9, somewhat closer to the larger disturbance level of N_{crit} = 1. Table I shows a summary of typical N_{crit} for different situations, offering a better grasp of this value's range under different flow conditions.

As can be observed from Fig. 1, there is a significant loss of performance (L/D decrease) as factor N_{crit} is reduced from 9 to 1. Also, it is clear the angle of attack (AOA) which maximises L/D, *i.e.* the optimum AOA, is influenced by the value of N_{crit} . Fig. 2 shows that, as expected, transition occurs closer to the leading edge for all angles of attack as N_{crit} decreases. Given the environment in which marine turbines operate, N_{crit} = 1 could be plausible for the present study.

TABLE I
TYPICAL N_{CRIT} VALUES (FOR REFERENCE). SOURCE: [13]

Situation	N_{crit} value
Sailplane	12-14
Motor glider	11-13
Clean wind tunnel	10-12
Average wind tunnel	9
Dirty wind tunnel	4-8

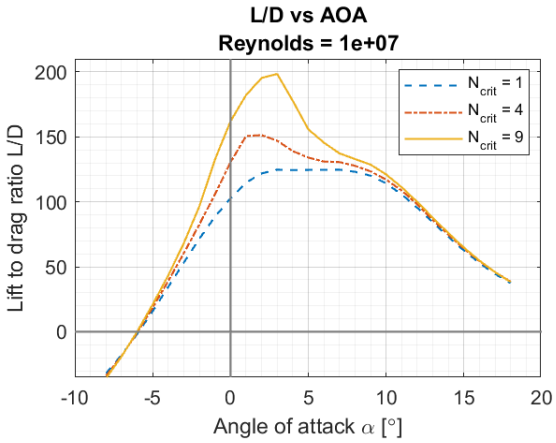

Fig. 1. N_{crit} influence on L/D vs AOA for Reynolds number of $1{\cdot}10^7$ – hydrofoil NACA 63-815.

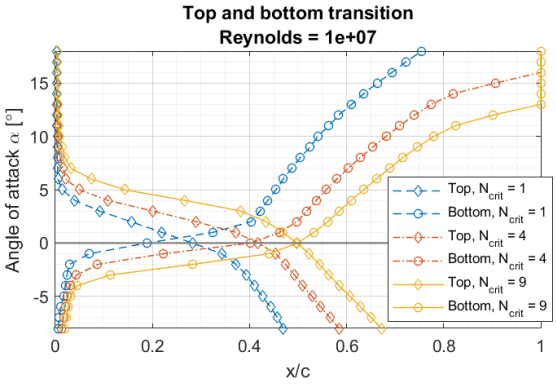

Fig. 2. N_{crit} influence on transition on the upper and lower foil surfaces at Reynolds number of $1{\cdot}10^7$ – hydrofoil NACA 63-815.

However, such a loss in performance was considered too dramatic and (hopefully) unrealistic. As such, N_{crit} = 4 was considered an appropriate value for simulating the marine turbines' operating conditions. From this point on, all data relative to foil performance is obtained with this parametric value. Results for the NACA 63-815 section can be seen in Fig. 3.

B. Design of reference turbine

1) Design method – lifting line theory-based method

The problem of finding the conditions under which a horizontal-axis turbine extracts the maximum power from a fluid stream is of major importance both in the wind and

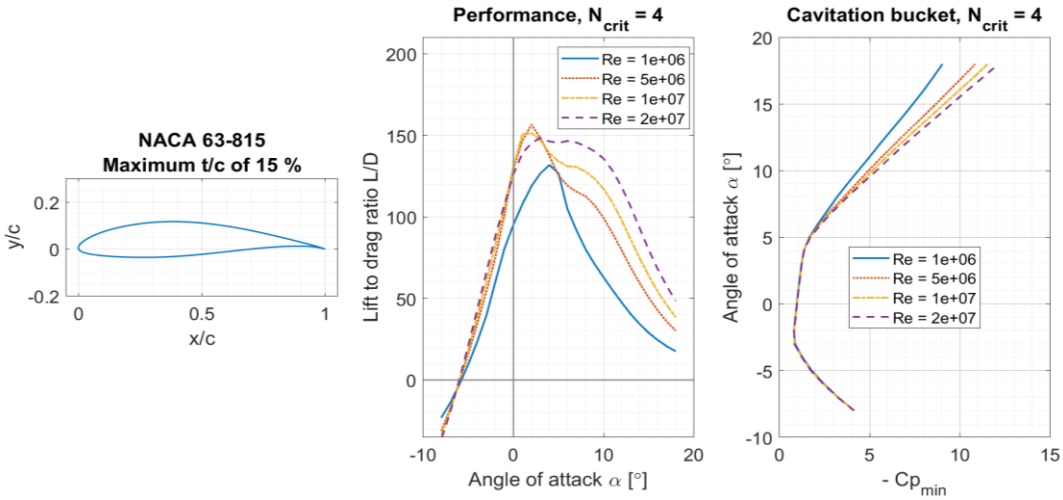

Fig. 3. Geometry of NACA 63-815 foil, numerical performance and cavitation bucket for N_{crit} = 4 – XFOIL data.

marine current fields. For rotors with blades of high aspect ratio, the lifting line theory offers a suitable model for the lifting action of the blades which inherently considers the finite number of blades. This theory was originally introduced by Prandtl et al. for wings and later adapted to propellers in the classical works of Betz, in 1919 [15] and Goldstein, in 1929 [16]. The lifting line model evolved to a well-established tool for the hydrodynamic design of marine propellers. Among others, this was due to the work of Lerbs in 1952 [17]. The method used for the present work applies the optimization of Betz to a horizontal-axis turbine modelled by lifting line theory. The calculation of the induced velocities due to a helicoidal vortex is based on the analytical expressions of the induction factor method (Lerbs, 1952 [17], Wrench et.al, 1965 [18]). The vortex lattice method (Kerwin et.al, 1986 [19]) is used for the numerical calculation of the principal value integral at the lifting line. For additional information see [10] and [11].

The specific method used in the current design effort is as follows: The values of optimum L/D are defined for each radial section r/R. From this specification, the optimum AOA and correspondent design lift coefficient $C_{l_{DES}}$ for each section are selected as input design variables. Using the classical optimization criterion of constant induced hydrodynamic pitch distribution, the optimum circulation distribution is calculated for a specified tip speed ratio TSR and a prescribed thrust coefficient C_T. The thrust coefficient is systematically varied to find the optimal value of the power coefficient C_P. The blade pitch and chord spanwise distributions $(\theta(r), c(r))$ follow from the hydrodynamic pitch and circulation distributions with the selected design angle of attack and lift coefficient, and they are the design output variables

2) Reference turbine design

The full-scale reference turbine is designed using the method based on lifting line theory, as described above. Table II presents the main design parameters of the full-scale turbine used as input for the lifting line routine. Rotor radius, hub depth and height and design conditions (TSR and U_0) are chosen to match previous studies [20]. As mentioned before, the blades of the reference turbine are comprised of hydrofoils NACA 63-824, 63-821, 63-818, 63-815 and 63-812. Table III and Fig. 4 show the reference foil section's geometry and spanwise distribution.

Table IV shows the results obtained from the lifting-line method, namely the chord, relative thickness, pitch and Reynolds number radial distributions at the design conditions of the full-scale reference turbine. Fig. 5 and Fig. 6 illustrate the reference turbine blade chord and pitch distribution, respectively.

TABLE II
FULL-SCALE TURBINE DESIGN PARAMETERS

Variable	Symbol		Value
Hub height to sea floor	h_0	m	15
Hub depth to mean sea level	d_0	m	15
Rotor diameter	D_T	m	20
Rated flow speed	U_0	m/s	2
Design tip speed ratio	TSR	-	6
Number of blades	-	-	3
Fluid density	ρ	kg/m^3	1025
Fluid vapour pressure	p_v	Pa	1670
Fluid kinematic viscosity	ν	m^2/s	$1.18 \cdot 10^{-6}$

TABLE III
REFERENCE TURBINE FOIL SECTION DISTRIBUTION

Span r/R [%]	Foil at section
20	NACA 63-824
30	NACA 63-821
45	NACA 63-818
75	NACA 63-815
100	NACA 63-812

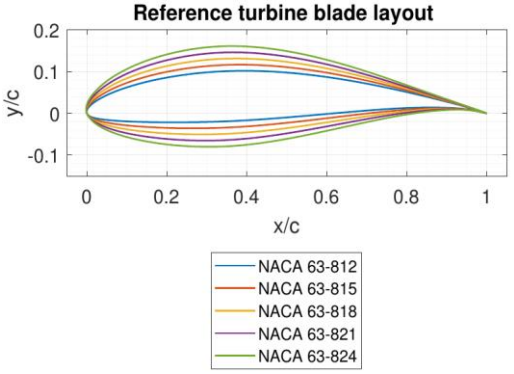

Fig. 4. Reference turbine blade section layout

TABLE IV
REFERENCE TURBINE DATA – TSR = 6, U_0 = 2 M/S

Span r/R [%]	Chord c/R [%]	Thickness t/c [%]	Pitch θ [°]	Reynolds Re [-]
20	15.0	24.0	24.4	$3.9 \cdot 10^6$
25	14.0	22.5	20.1	$4.2 \cdot 10^6$
30	13.2	21.0	17.0	$4.5 \cdot 10^6$
35	12.5	19.5	14.7	$4.9 \cdot 10^6$
40	11.7	18.7	13.0	$5.1 \cdot 10^6$
45	11.0	18.0	11.5	$5.3 \cdot 10^6$
50	10.3	17.6	10.4	$5.5 \cdot 10^6$
55	9.6	17.1	9.3	$5.6 \cdot 10^6$
60	8.9	16.6	8.4	$5.6 \cdot 10^6$
65	8.2	16.1	7.5	$5.6 \cdot 10^6$
70	7.6	15.6	6.8	$5.5 \cdot 10^6$
75	7.1	15.0	6.2	$5.5 \cdot 10^6$
80	6.6	14.6	5.8	$5.5 \cdot 10^6$
85	6.0	14.1	5.5	$5.3 \cdot 10^6$
90	5.3	13.6	5.2	$4.9 \cdot 10^6$
95	4.0	12.8	5.0	$3.9 \cdot 10^6$
100	0.7	12.0	4.9	$5.2 \cdot 10^5$

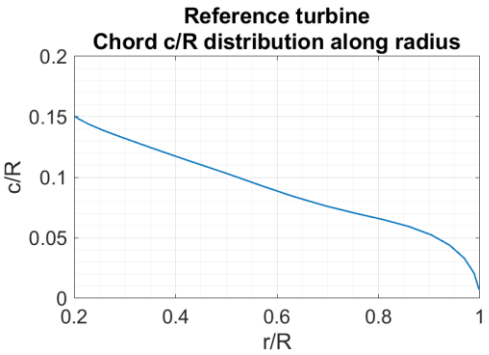

Fig. 5. Reference turbine blade chord distribution

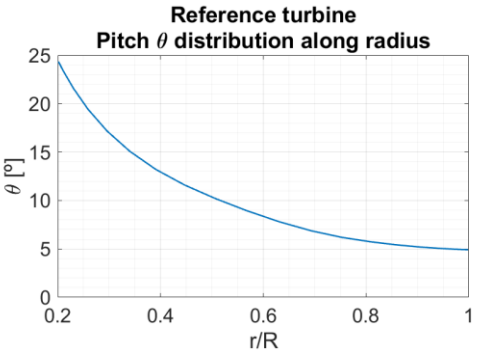

Fig. 6. Reference turbine blade' pitch distribution

shows the turbine power coefficient C_P as function of the TSR.

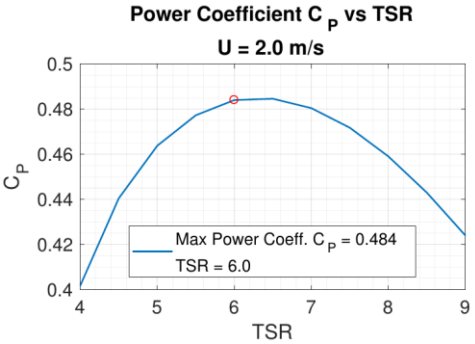

Fig. 7. Reference turbine power coefficient as function of TSR

Fig. 9 displays the lifting line predictions of the full-scale reference turbine C_P vs TSR, together with experimental data of the Bahaj et al model turbine [7] and lifting line predictions for the model turbine [21]. Reasonable agreement is obtained between experimental and lifting line data for the model turbine, with a 4% difference on the maximum C_P, albeit at slightly different TSR values.

Fig. 9 shows the lifting line routine predicts a higher C_P of 0.483 for the full-scale reference turbine than for the Bahaj model turbine (C_P is higher by 10%), at the same TSR. This larger power coefficient is attributed to scale-effects; On a full-scale turbine, the operational Reynolds number is higher, which is favourable in terms of L/D on the blades because, usually, at higher Re foils exhibit higher L/D ratios.

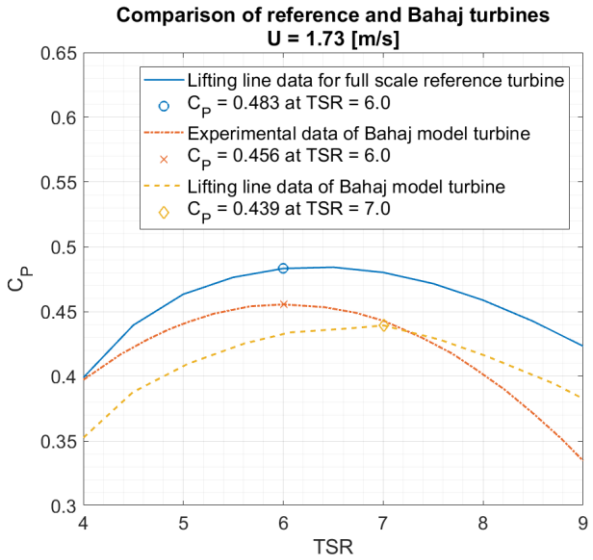

Fig. 9. Reference full scale turbine lifting line data, experimental data of model turbine [7] and lifting line data of model turbine [21] – power coefficient C_P in function of TSR

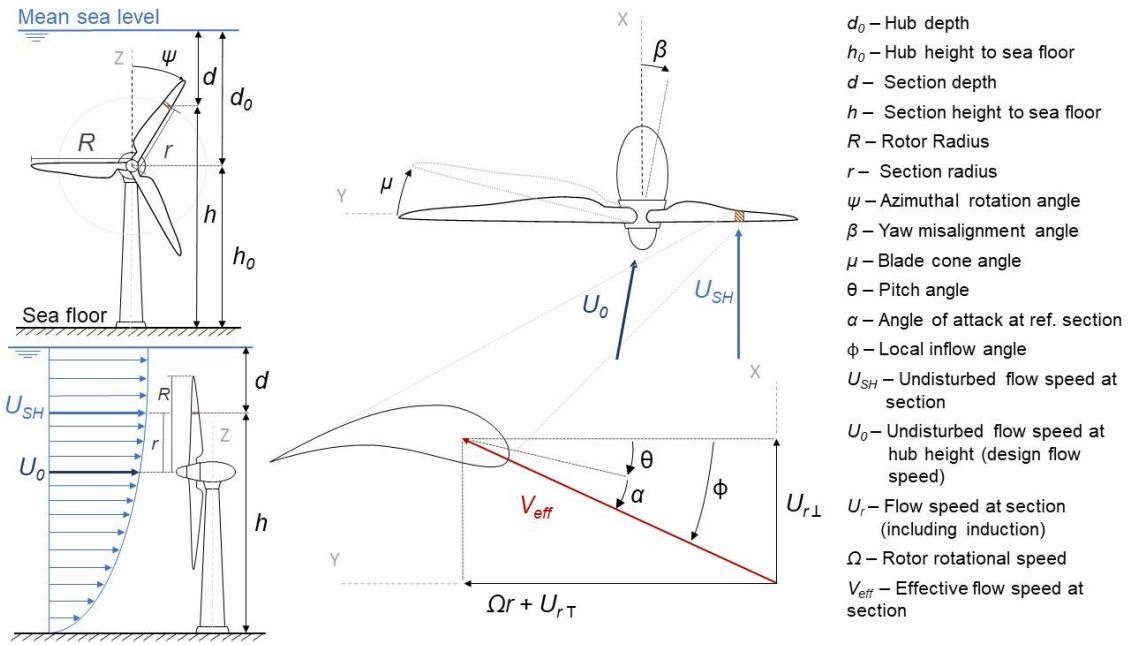

Fig. 8. *Left*: Marine turbine schematic; *Centre*: reference blade section (at approx. $r/R = 75\%$) view and velocities diagram; *Right*: variables designation

C. Operating curves

In order to obtain the operating curves of the full-scale reference turbine, *i.e.* the cavitation number σ and angle of attack (*AOA* or α) felt on the section along the blade span as it rotates azimuthally (Ψ = 0° to 180°, see Fig. 8), an analytical method based on [22] is adapted. This method employs an analytical expression to calculate the probability of perturbations to the operational blade-section AOA, considering the combined influence of non-uniform velocity profile (induced by wall shear), yaw-misalignment and ambient turbulence intensity. For simplicity, in the present article, flow stream turbulent perturbations on effective flow speed at the section V_{eff} are not taken into account. The calculation of V_{eff} and the local inflow angle ϕ are described in the following subsections and Fig. 8 shows the variables used in the present formulation.

1) Effective flow speed V_{eff} calculation

The effective flow speed V_{eff} at the blade section is calculated by:

$$V_{eff} = \sqrt{U_{r\perp}^2 + (\Omega r + U_{r\top})^2} \tag{1}$$

where Ur⊥ and Ur⊤ are defined as follows:

$$U_{r\perp} = U_{SH} \cdot \cos\beta \cdot (1 - a - K \cdot \sin\Psi) \tag{2}$$

$$U_{r\top} = U_{SH} \cdot \sin\beta \cdot \cos\Psi \tag{3}$$

where β is the yaw misalignment angle, a is the axial induction factor, Ψ is the azimuthal rotation angle, U_{SH} is the flow speed at the section (due to flow shear, *SH*, see Fig. 8) and K is the yaw misalignment factor, a parameter that depends on the radial coordinate, the yaw misalignment and the axial induction factor:

$$K = \frac{15\pi}{32} \cdot \frac{r}{R} \cdot \left(\frac{\beta(0.6a + 1)}{2}\right) \tag{4}$$

Marine current shear is approximated by the logarithmic shear law:

$$U_{SH} = U_0 \frac{\ln h - \ln z_r}{\ln h_0 - \ln z_r} \tag{5}$$

where h is the section height, U_0 is the undisturbed flow speed at the hub height (see Fig. 8) and z_r is the roughness factor. This value is taken as 3 cm, according to [23], [24] and [25]. The section height is calculated as $h = h_0 \cdot r \cdot \cos\Psi \cos\mu$, where μ is the rotor pre-bend or blade cone angle. The axial induction factor a used in these calculations is an output of the lifting line routine, and thus the final result of this procedure is a combination of both analytical and computational methods. The tangential induction factor is not included as it is considered negligible [22].

2) Local inflow angle ϕ calculation

Using the same logic as for V_{eff}, the local inflow angle ϕ calculation is based on an analytical method [22] and is calculated as follows:

$$\phi = \arctan\left(\frac{\cos\beta \cdot (1 - a - K \cdot \sin\Psi)}{\lambda_r - \sin\beta\cos\Psi}\right) \tag{6}$$

Where λ_r is the local TSR at section r:

$$\lambda_r = \frac{\Omega \cdot r}{U_{SH}} = \frac{\Omega \cdot r}{U_0} \cdot \frac{\ln h_0 - \ln z_r}{\ln h - \ln z_r} \tag{7}$$

The AOA is finally calculated as the difference between the local inflow angle ϕ and the local pitch angle θ: $\alpha = \phi - \theta$. For this calculation, the computational value (obtained from the lifting line routine) of the axial induction factor a is used as well. Though the influence of yaw misalignment and cone angle on both V_{eff} and ϕ may be studied with the analytical approach, the present study considers no yaw-misalignment and no cone angle ($\beta = \mu$ = 0°).

Fig. 10 displays the operating curves of the full-scale reference turbine/ The cavitation number is calculated through equation (8):

$$\sigma = \frac{p_\infty - p_v}{1/2 \cdot \rho\, V_{eff}^2} \tag{8}$$

where p_∞ is the undisturbed flow pressure, $p_\infty = p_{hyd} + p_{atm}$, with $p_{hyd} = \rho g d$. The cavitation number varies significantly along the span, increasing towards the root of the blade. This increase in cavitation number is readily explained by the smaller effective velocities at inner stations of the blade, due to the smaller distance to the centre of the rotor. Fig. 10 also shows the AOA variation induced by the marine current shear (*i.e.* non-homogeneous velocity profile) is in the order of $d\alpha \sim 1°$ throughout the blade span, although slightly larger towards the tip of the blade. A larger AOA variation at outboard regions is explained by the large height variation and hence axial velocity component (U_{SH}) variation at a given blade section per rotor revolution, compared to inboard blade stations.

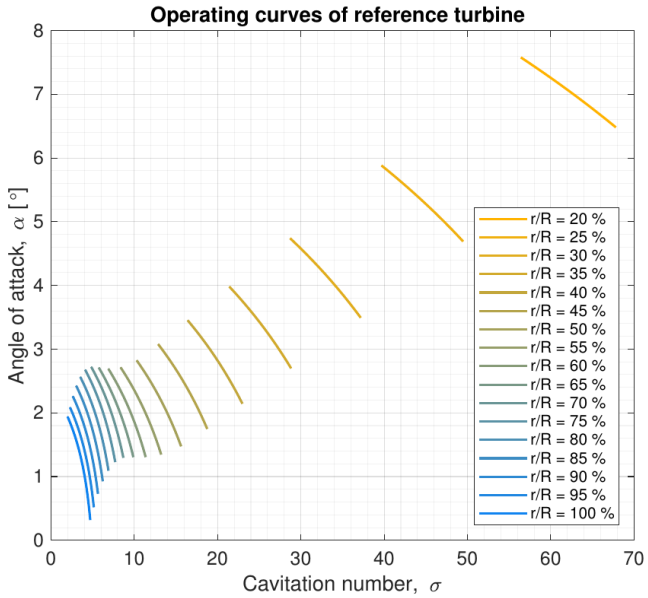

Fig. 10. Operating curves of blade sections along the span - cavitation number vs AOA at section – TSR = 6, U_0 = 2 m/s

At this point it is noted the cavitation number values depend on the undisturbed flow pressure and main turbine characteristics (*i.e.* TSR, water depth, etc), but not explicitly on the foil section of the turbine blades. In other words, this means the cavitation number values obtained for the full-scale reference turbine will be (nearly) the same for the full-scale final, redesigned turbine.

Instead, the influence of the foil sections on the turbine's potential to cavitate is seen on the cavitation margin, calculated simply as the difference between the cavitation number (eq. (8)) and the minimum pressure coefficient $-C_{p_{min}}$ occurring over the foil surface. The minimum pressure coefficient depends strongly on the foil geometry and operating AOA, but since the HACT dedicated foils used on the redesigned turbine (explained in section III) were designed to restrict $-C_{p_{min}}$, it is expected the cavitation margin of the redesigned full-scale HACT is at least as large as for the reference, full-scale turbine. For more information on the cavitation margin and a comparison between reference and HACT-specific foils, the reader is referred to [8],[9].

III. Redesigned Turbine

In this section a redesigned turbine is considered, with HACT-dedicated IST-MT1-XX foils. The geometry of the redesigned turbine is obtained in a two-step approach: firstly, a hydrodynamically optimized turbine is established by employing the lifting line routine mentioned in B.1); secondly, adjustments are made to the turbine blades' chord and pitch in order to obtain a new planform design which complies with a structural criterion.

D. Redesigned turbine section data

The hydrofoils that comprise the various sections of the blades of the redesigned turbines foils optimized for employment in marine current turbines - the IST-MT1-XX series. Table V details the foil distribution along the blade span of the redesigned turbine, as well as the Reynolds number at the respective section, and Fig. 11 displays the geometry of the IST-MT1-XX foils.

TABLE V
REDESIGNED TURBINE BLADE SECTION DISTRIBUTION

Span r/R [%]	Foil at section
20	IST-MT1-24
30	IST-MT1-21
45	IST-MT1-18
75	IST-MT1-15
100	IST-MT1-12

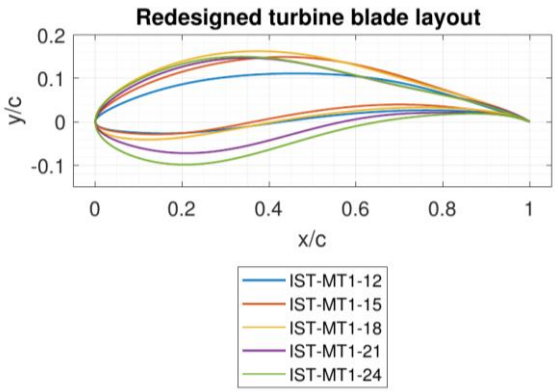

Fig. 11. IST-MT1-XX foil geometry

E. Hydrodynamically optimized turbine

The first step in obtaining the redesigned turbine is carried out with the lifting line method mentioned in B.1) and considering only hydrodynamic performance, *i.e.* only C_P maximization is strived for. The lifting line routine results for blade chord and pitch distribution are shown in figures Fig. 14 and Fig. 15. The hydrodynamically optimized turbine yields a power coefficient of 0.486 at design conditions, TSR = 6 and U_0 = 2 m/s, and slightly larger $C_P$at higher TSRs.

Comparing with the reference full-scale turbine, at design conditions an increase of 0.3% is verified, which is a marginal improvement; more significantly, there is reduction in chord of up to 41% at r/R = 45%. The chord size reduction is explained by the difference in design lift

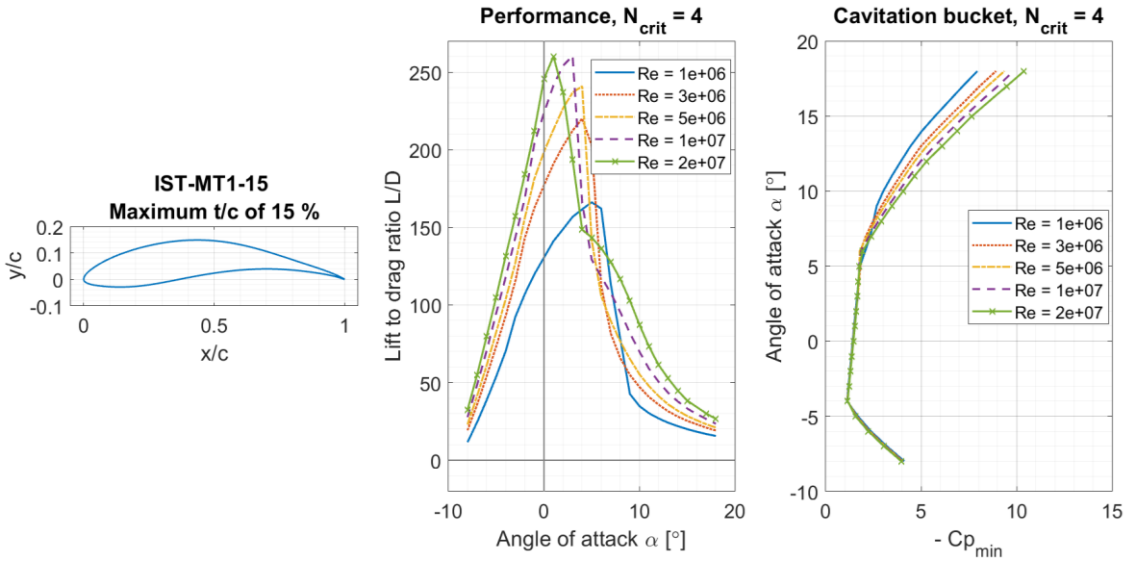

Fig. 12. IST-MT-15 hydrofoil, performance and cavitation bucket - data obtained with XFOIL

coefficient $C_{l_{DES}}$ of the NACA 63-8XX and IST-MT1-XX foil series. From a theoretical point of view, the (hydrodynamic) loading on a given blade section is proportional to the product of lift coefficient by chord, $C_l.c$. Particularly in the lifting method employed, and since the design TSR, rotor diameter and rated flow speed are kept constant, the optimum circulation, and hence loading distribution, will be very similar for both turbines. Since the design lift coefficient $C_{l_{DES}}$of the IST-MT1-XX foils is significantly higher than for the NACA 63-8XX series, the same local loading is obtained with a significantly smaller chord.

1) On the performance of the hydrodynamically optimized turbine

When analysed with XFOIL, the HACT-dedicated foils IST-MT1-XX display higher L/D values than the NACA 63-8XX series foils for all Reynolds numbers considered as illustrated in Fig. 3 and Fig. 12 (refer to [8],[9] for complete data). However, this higher performance does not render a significant increase in power coefficient C_P between the reference and redesigned turbines as large as could be expected. This is most likely due to two reasons:

1) The full-scale reference turbine is already a theoretically optimized version of an existing model turbine;
2) As mentioned before, with the design method employed the optimal blade chord is inversely proportional to the value of the lift coefficient C_L at each section, which is in turn dependent on the specific hydrofoil. However, and as detailed in [8],[9], the IST-MT1-XX hydrofoils are optimized for the Reynolds number corresponding to the full-scale reference turbine at the section where each hydrofoil is employed. Having blade sections with smaller chords leads to a lower Reynolds number at each section, thus resulting in the IST-MT1-XX foils operating at "off-design" or non-optimal conditions in the hydrodynamically optimized turbine, which explains why the increase in C_P is only marginal when compared to the reference turbine.

From Fig. 12 it is possible to observe that, if operating at Re = $5{\cdot}10^6$ instead of Re = $3{\cdot}10^6$, the IST-MT1-15 renders an L/D of 240 instead of 220, for the same angle of attack of $\alpha = 4°$, and even higher L/D values for Re = $1{\cdot}10^7$ at an AOA of 3°. This explains why the redesigned turbine yields higher values of C_P for larger TSR than at design condition: as TSR increases, the Reynolds number increases as well and the AOA decreases, resulting in a combined effect (*Re* increasing and AOA decreasing) which ultimately increases the hydrofoil performance, *i.e.* L/D. During the design [8],[9] of the IST-MT1-XX foils, the Reynolds number was not updated to take into account the increase in design C_L and its subsequent effect on the blades' chord for a (nearly) constant, optimum loading.

F. Strength considerations

A simplified strength analysis is carried out for the full-scale turbines. The strength analysis employs Euler-Bernoulli beam theory for the calculation of blade stresses, where it is assumed turbines' blades are solid and made from a homogeneous material. The analysis considers only steady-state regime and uniform inflow conditions, *i.e.* it is assumed the hydrodynamic and structural forces are in static equilibrium. The total stress is calculated using the von Mises criteria:

$$\sigma_{VM} = \sqrt{(\sigma_B + \sigma_C)^2 + 3 \cdot \tau^2} \tag{9}$$

where σ_B is the normal stress due to the bending moment, σ_C is the normal stress due to centrifugal forces and τ is shear stress resulting from shear forces. From these three components, stresses arising from the flap-wise bending moment σ_B are the most relevant.

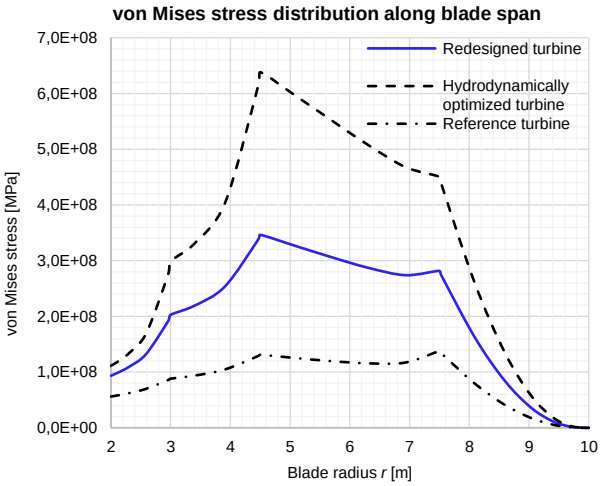

Fig. 13. von Mises stress distribution along the blade span

The resulting von Mises stress along the blade span are shown in Fig. 13. It is clear the hydrodynamically optimized turbine experiences very large (von Mises) stress values, approximately 6 times the value obtained for the reference turbine at a radial position $r = 4.5\ m$. This is a direct consequence of the significant chord reduction. The normal stress arising from the bending moment is calculated with:

$$\sigma_B = \frac{M.y}{I_{xx}} \tag{10}$$

where M is the bending moment about the neutral axis, y is the distance perpendicular to the neutral axis, and I_{xx} is the second moment of area about the neutral axis. For horizontal axis turbines, the dominant component of the bending moment is in the flap-wise direction, and since we are considering solid blade sections, the following approximations hold:

$$y \propto c \ , \quad I_{xx} \propto c^4 \tag{11}$$

Since the loading distribution is similar for both turbines, the bending moment at a given blade section should also be comparable. Under these approximations, one can expect the stress will be inversely proportional to

the cube of the blade chord. At a radial position of $^{r}/_{R} = 0.45$ the hydrodynamically optimized turbine chord is approximately 60% of the reference turbine, and as such we have:

$$c_{HYD}(0.45) \approx 0.6 c_{REF}(0.45) \quad \rightarrow$$
$$\sigma_{B_{HYD}}(0.45) \approx \frac{1}{0.6^3}\sigma_{B_{REF}}(0.45) \approx 5\sigma_{B_{REF}}(0.45) \tag{12}$$

which is in line with the results shown in Fig. 13.

G. *Final redesigned turbine*

In order to reduce the maximum stress values occurring along the blades and in order to obtain a feasible HCT design, the chord is increased with respect to the hydrodynamically optimized turbine. The chord distribution of the final redesigned turbine is obtained through a weighted interpolation of both the reference and the hydrodynamically optimized turbines' chord distribution:

$$c_{REDES.}(r) = w \cdot c_{REF.}(r) + (1 - w) \cdot c_{HYD}(r) \tag{13}$$

where the weighting value $w = 0.328$ is used such that the maximum stress obtain over the blade span of the redesigned turbine is $Max(\sigma_{REDES}) = 345\ MPa$, as shown in Fig. 13. This particular stress value is somewhat arbitrarily chosen to correspond to the yield stress of Nikalium, typically applied in marine propellers [26], employing a safety factor *FS*=2.

For consistency with the updated chord distribution, the blade pitch is also adjusted. At each radial station, the pitch angle is altered to maintain the same load factor as for the hydrodynamically optimized turbine. This is done by obtaining the operational AOA of hydrofoils IST-MT1-XX for the Reynolds number and lift coefficient C_L verified at each section. The new pitch distribution is then calculated by subtracting the obtained AOA from the pitch angle verified at the same section for the hydrodynamically optimized turbine, expressed by:

$$C_{l_{REDES}} = C_{l_{REDES}} \cdot \frac{c_{HYD}}{c_{REDES}} \tag{14}$$

$$\theta_{REDES}(r) = \theta_{HYD}(r) + \alpha(r)|_{C_{l_{HYD}}} - \alpha(r)|_{C_{l_{REDES}}} \tag{15}$$

The pitch and chord distributions of the final, redesigned turbine are given in Table VI, together with the chord reduction with respect to the reference turbine. Fig. 14 and Fig. 15 show the planform of the 3 full scale turbines, including the final redesigned turbine, the reference turbine and the hydrodynamically optimized turbine. Regarding the chord spanwise distribution, Fig. 14 shows the redesigned turbine has chord values that are smaller than the reference turbine and larger than the hydrodynamically optimized turbine, with a smooth spanwise distribution. Compared to the reference turbine, the final redesigned turbine shows a maximum chord reduction of 27%, at *r*/*R* = 45%. As for the pitch angle, Fig. 15 also shows a smooth spanwise distribution, with the pitch of the final redesigned turbine having larger value than the hydrodynamically optimized turbine. This is expected as the chord increase leads to lower operational lift coefficient, thus lower angle of attack, and hence larger blade pitch angle. It is hard to make a direct comparison between the pitch distribution of the reference turbine and the final redesigned turbine as the two rotors employ different foil sections, and thus different optimum AOA at each blade station.

Fig. 16 displays the variation of the power coefficient with TSR, for both the reference and the final redesigned turbine. It can be seen that both turbines yield very similar power coefficients over the investigated TSR range, which confirms that the final redesigned turbine is not only a feasible rotor form a structural point of view but also maintains the performance of the reference turbine.

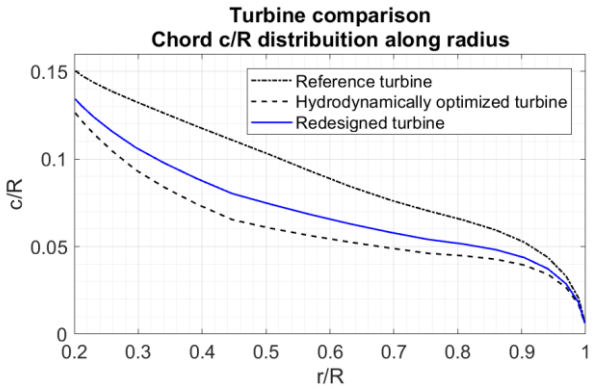

Fig. 14. Redesigned turbine blade chord distribution

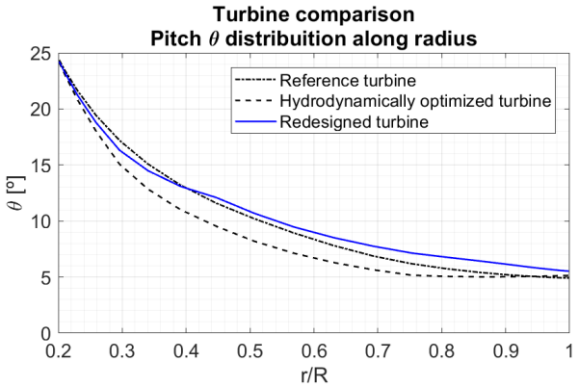

Fig. 15. Redesigned turbine blade pitch distribution

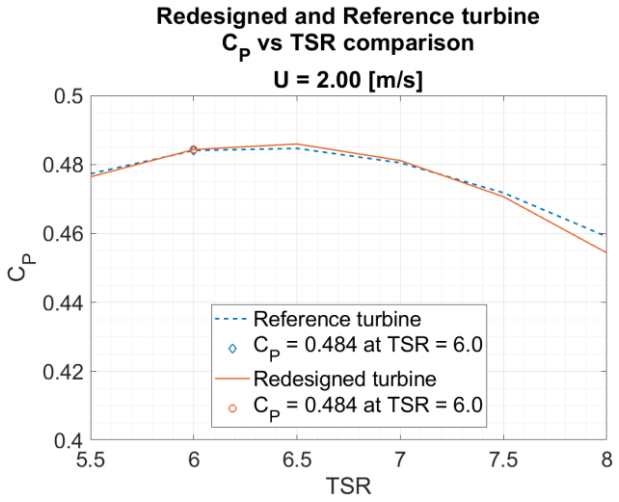

Fig. 16. Redesigned and reference turbine C_P vs TSR comparison

TABLE VI
REDESIGNED TURBINE DATA – TSR = 6, U_0 = 2 M/S

Span r/R [%]	Chord c/R [%]	Thickness t/c [%]	Pitch θ [°]	Reynolds Re [-]	Chord reduction [%]
20	13.4	24.0	24.2	$3.5 \cdot 10^6$	10.7
25	11.8	22.5	19.5	$3.5 \cdot 10^6$	15.6
30	10.6	21.0	16.1	$3.6 \cdot 10^6$	20.0
35	9.6	19.5	14.2	$3.7 \cdot 10^6$	23.0
40	8.8	18.7	12.9	$3.8 \cdot 10^6$	25.5
45	8.0	18.0	12.0	$3.9 \cdot 10^6$	27.5
50	7.5	17.6	10.8	$4.0 \cdot 10^6$	27.5
55	7.0	17.1	9.8	$4.1 \cdot 10^6$	26.9
60	6.6	16.6	9.0	$4.1 \cdot 10^6$	26.0
65	6.2	16.1	8.3	$4.2 \cdot 10^6$	25.0
70	5.8	15.6	7.7	$4.2 \cdot 10^6$	24.0
75	5.4	15.0	7.2	$4.2 \cdot 10^6$	23.2
80	5.2	14.6	6.8	$4.3 \cdot 10^6$	21.4
85	4.9	14.1	6.5	$4.3 \cdot 10^6$	19.3
90	4.4	13.6	6.2	$4.1 \cdot 10^6$	17.0
95	3.5	12.8	5.8	$3.4 \cdot 10^6$	14.4
100	0.6	12.0	5.5	$6.4 \cdot 10^5$	11.3

Finally, Table VII contains a comparison of values of lift coefficient, chord, angle of attack and Reynolds number between the reference, hydrodynamically optimized and final redesigned turbines at r/R = 75%. This serves to better illustrate the compromise underpinning the current design effort. One may see how the lift coefficient is (nearly) inversely proportional to the chord, and how the Reynolds number changes accordingly. Table VII also shows how the final, redesigned turbine represents a feasible compromise between the reference turbine, with 2reference" foils, and the somewhat unrealistic hydrodynamically optimized turbine, employing HCT dedicated foils.

TABLE VII
COMPARISON OF VALUES AT R/R = 75% BETWEEN THE REFERENCE, HYDRODYNAMICALLY OPTIMIZED AND FINAL REDESIGNED TURBINE

Variable	Reference turbine	Hydrodynamic optimized turbine	Final redesigned turbine
Lift coefficient, C_L	0.943	1.466	1.253
Chord, c [m]	0.708	0.463	0.543
Angle of attack, AOA [°]	2.047	2.905	0.859
Reynolds number, Re	$5.5 \cdot 10^6$	$3.6 \cdot 10^6$	$4.2 \cdot 10^6$

IV. CONCLUSIONS

The present study addressed the planform design of full-scale marine current turbines using of a lifting line theory-based method. Both a reference turbine and a redesigned turbine are presented; the first uses "reference" NACA 63-8XX foils whereas the latter employs dedicated marine turbine foils IST-MT1-XX.

In a preliminary step, the effect of the N_{crit} factor on foil performance is studied, resulting in the observation that the variation of this parameter not only alters the performance for all Reynolds numbers tested but also the optimum AOA at which peak performance occurs. Along with these changes, the variation of this factor has a very noticeable effect on the chord-wise location of transition. It is concluded that including the influence of the N_{crit} factor may be of paramount importance to successfully mimic real the operating conditions.

The full-scale reference turbine is based on the work published by Bahaj et al and is designed through a routine based on lifting line theory. A power coefficient of 0.484 is obtained at design conditions of TSR = 6 and U_0 = 2m/s.

Subsequently, a so-called hydrodynamically optimized turbine is designed using the same methodology and incorporating the HACT-dedicated hydrofoils IST-MT-XX in its blades. This hydrodynamically optimized turbine yields a power coefficient of C_P of 0.486 at the design conditions of TSR = 6 and U = 2 m/s, which represents an increase in C_P of 0.3% relative to the performance of the reference turbine at design conditions. For the off-design conditions of TSR = 6.5, the increase in C_P is of 1.16%. Along with this modest increase in power coefficient, a chord reduction of up to 41% is obtained.

The geometry of the hydrodynamically optimized turbine is finally readjusted to accommodate the stresses at design condition. The chord distribution of the final, redesigned turbine is obtained through a weighted interpolation between the reference and the hydrodynamically optimized turbine blade chord. The pitch distribution is then adjusted to maintain the same load factor as for the hydrodynamically optimized turbine.

The redesigned turbine:

- successfully lowers stresses along the blades, complying with a safety factor of 2 if the material Nikalium is employed;
- maintains the performance (C_P = 0.484 at TSR = 6 and U_0 = 2 m/s) of the reference turbine;
- reduces chord size up to 27.5%.

As future work, the integrated optimization of hydrofoils and blades should be considered a priority. Updating the chord size as new values of lift coefficient are obtained for each optimized hydrofoil would result in the readjustment of the Reynolds number at the section. This type of procedure would avoid the application and off-design operation of hydrofoils optimized for a different Reynolds number when the blade design is finalized. As a final remark, it is noted that a more encompassing structural analysis should accompany the process of blade optimization, as the current study employs a very simple methodology.

ACKNOWLEDGEMENT

This work was supported by FCT/MCTES (PIDDAC) through project UID/EEA/50009/2019.

REFERENCES

[1] U.S. Energy Information Administration, "Annual Energy Outlook 2011," 2011.

[2] R. Pelc and R. M. Fujita, "Renewable energy from the ocean," *Mar. Policy*, vol. 26, no. 6, pp. 471–479, 2002.

[3] The Executive Committee of Ocean Energy Systems, "An overview of Ocean Energy activities in 2017 - Annual Report," 2017.

[4] Z. Zhou, M. Benbouzid, J.-F. Charpentier, F. Scuiller, and T. Tang, "Developments in large marine current turbine technologies – A review," *Renew. Sustain. Energy Rev.*, vol. 71, pp. 852–858, May 2017.

[5] K. W. Ng, W. H. Lam, and K. C. Ng, "2002-2012: 10 Years of Research Progress in Horizontal-Axis Marine Current Turbines," *Energies*, vol. 6, no. 3, pp. 1497–1526, 2013.

[6] M. J. Khan, G. Bhuyan, M. T. Iqbal, and J. E. Quaicoe, "Hydrokinetic energy conversion systems and assessment of horizontal and vertical axis turbines for river and tidal applications: A technology status review," *Appl. Energy*, vol. 86, no. 10, pp. 1823–1835, 2009.

[7] A. S. Bahaj, A. F. Molland, J. R. Chaplin, and W. M. J. Batten, "Power and thrust measurements of marine current turbines under various hydrodynamic flow conditions in a cavitation tunnel and a towing tank," *Renew. Energy*, vol. 32, no. 3, pp. 407–426, 2007.

[8] F. Espenica, "Design and Optimization of Hydrofoils tailored for Marine Current Turbines,", M.Sc. thesis, Instituto Superior Técnico, Lisbon, 2018.

[9] F. Espenica, R. B. Santos Pereira, G. de Oliveira, J. Baltazar, and J. A. C. Falcão de Campos, "Design and optimization of hydrofoils tailored for marine current turbines," Lisbon,submitted to *EWTEC 2019*, 2019.

[10] J. Machado, J. Baltazar, and J. A. C. Falcão de Campos, "Hydrodynamic Design and Analysis of Horizontal Axis Marine Current Turbines With Lifting Line and Panel Methods," in *OMAE*, 2011, p. 13.

[11] J. A. C. Falcão de Campos, "Hydrodynamic Power Optimization of a Horizontal Axis Marine Current Turbine with Lifting Line Theory," in *ISOPE*, 2007, pp. 307–313.

[12] M. Drela, "XFOIL: An Analysis and Design System for Low Reynolds Number Aerodynamics," 1989, vol. 54, no. December.

[13] M. Drela and H. Youngren, "XFOIL - Subsonic airfoil development system," 2013. [Online]. Available: http://web.mit.edu/drela/Public/web/xfoil/. [Accessed: 04-Sep-2018].

[14] G. B. Schubauer and H. K. Skramstad, "Laminar-Boundary-Layer Oscillations and Transition on a Flat Plate," Washington DC, USA, 1948.

[15] A. Betz, "Schraubenpropeller mit geringstem Energieverlust," *Göttinger Nachrichten*, no. 1919, p. 2018, 1919.

[16] S. Goldstein, "On the Vortex Theory of Screw Propellers," *Proc. R. Soc. A Math. Phys. Eng. Sci.*, vol. 123, no. 792, pp. 440–465, 1929.

[17] H. W. Lerbs, "Moderately Loaded Propellers with a Finite Number of Blades and an Arbitrary Distribution of Circulation," *Trans. Soc. Nav. Archit. Mar. Eng.*, vol. 60, no. 1952, pp. 73–123, 1952.

[18] W. B. Morgan and J. W. Wrench, "Some computational aspects of propeller design," *Methods Comput. Phys.*, vol. 4, pp. 301–331, 1965.

[19] J. E. Kerwin, W. B. Coney, and C. Hsin, "Optimum Circulation Distributions for Single and Multi-component Propulsors," in *American Towing Tank Conference, 21st*, 1986.

[20] Y. L. Young, M. R. Motley, and R. W. Yeung, "Three-Dimensional Numerical Modeling of the Transient Fluid-Structural Interaction Response of Tidal Turbines," *J. Offshore Mech. Arct. Eng.*, vol. 132, no. 1, p. 011101, 2010.

[21] J. Baltazar and J. A. C. Falcão de Campos, "Hydrodynamic Analysis of a Horizontal Axis Marine Current Turbine With a Boundary Element Method," *J. Offshore Mech. Arct. Eng.*, vol. 133, no. 4, p. 041304, 2011.

[22] R. B. Santos Pereira, G. De Oliveira, W. A. Timmer, and E. Quaeghebeur, "Probabilistic Design of Airfoils for Horizontal Axis Wind Turbines," p. 10, 2018.

[23] W. D. Grant, "THE CONTINENTAL-SHELF BOTTOM BOUNDARY LAYER," pp. 265–305, 1986.

[24] A. D. Heathershaw and D. N. Langhorne, "Observations of Near-bed Velocity Profiles and Seabed Roughness in Tidal Currents Flowing over Sandy Gravels," pp. 459–482, 1988.

[25] X. Ke, M. B. Collins, and S. E. Poulos, "Coastal ISummer Velocity Structure and Sea Bed Roughness," vol. 10, no. 3, pp. 702–715, 2014.

[26] S. M. Propulsion, "Nikalium Technical Sheet." [Online]. Available: http://www.smpropulsion.com/technical/pdfs/Nikalium alloy NL.pdf.